

The Effect of Amino Acids on the Fenton and photo-Fenton Reactions in Cloud Water: Unraveling the Dual Role of Glutamic Acid

Peng Cheng^{1,2}, Gilles Mailhot^{1,3}, Mohamed Sarakha¹, Guillaume. Voyard¹, Daniele Scheres Firak⁴, Thomas Schaefer⁴, Hartmut Herrmann⁴, Marcello Brigante^{1}*

¹ Université Clermont Auvergne, CNRS, Institut de Chimie de Clermont-Ferrand, F-63000
Clermont–Ferrand, France.

² Department of Environmental Engineering, School of Resources and Environmental
Science, Wuhan University, 430079, PR China

³ Université Clermont Auvergne, CNRS, Laboratoire de Météorologie Physique (LaMP), F-
63000 Clermont–Ferrand, France.

⁴ Atmospheric Chemistry Department (ACD), Leibniz- Institute for Tropospheric Research
(TROPOS), 04318 Leipzig, Germany

*Corresponding author:

Marcello Brigante (Marcello.Brigante@uca.fr)

ABSTRACT

In this work, Glutamic acid (Glu) was selected as a model amino acid (AAs) to investigate its complexation with Fe(III) and Fe(II), focusing on its impact on the Fenton reaction and the photolysis of Fe(III) in cloud aqueous phase. Glu was found to enhance the rate constant for the reaction of Fe(II)-Glu with H₂O₂ to $1.54 \pm 0.13 \times 10^4 \text{ M}^{-1} \text{ s}^{-1}$, which is significantly higher than that of classic Fenton reactions ($\sim 50\text{-}70 \text{ M}^{-1} \text{ s}^{-1}$). In contrast, the photolysis quantum yield of Fe(III)-Glu complex was determined to be 0.037 under solar simulated irradiation, largely lower than Fe(III)-hydroxy complexes (0.216). In the overall process (Fenton or Fe(III) photolysis), it was found that $\bullet\text{OH}$ formation decreased in the presence of Glu. Additionally, the fate of Glu in the presence of Fe(III) was investigated as well as the oxidation process (driven by $\bullet\text{OH}$ and ligand-to-metal charge transfer (LMCT) reaction) led to the formation of short-chain carboxylic acids and ammonium under simulated solar light. Interestingly, these two processes generated different primary short-chain carboxylic acids, indicating distinct mechanisms. This study provides valuable insights into the role and fate of amino acids in atmospheric chemistry, helping to further understand their impact on atmospheric processes.

KEYWORDS: Glutamic acid, Fenton, hydroxyl radical, oxidant capacity, atmospheric composition

SYNOPSIS

This study investigates the complexation of Fe(II) and Fe(III) with glutamic acid under cloud water conditions and the effect on Fenton and photo-Fenton reactions, hydroxyl radical formation, and their impact on amino acid oxidation.

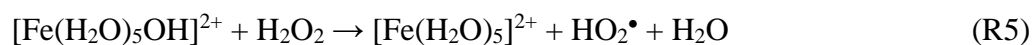
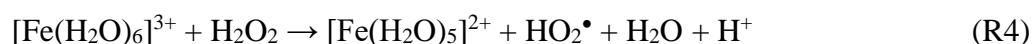
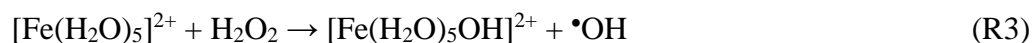
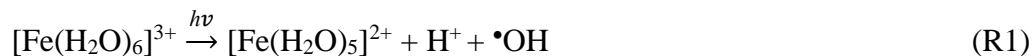
1. INTRODUCTION

The Earth's atmosphere is a dynamic system in which different phases, including gases, aerosol particles, water droplets, and ice particles, are all engaged in complex chemical interactions that continually modify the atmospheric chemical composition (Bianco et al., 2020; Kanakidou et al., 2018). Among these, the cloud aqueous phase stands out as a critical reactive system, encompassing gaseous, liquid, and solid components. In recent years, intensified research efforts have centered on unraveling the composition of atmospheric cloud waters, significantly advancing our comprehension of multiphase chemistry within the atmosphere (Bianco et al., 2018). Common components identified in both aerosols and cloud water include inorganic ions, transition metal ions (TMI) such as iron (Angle et al., 2021; Bianco et al., 2017), and organic carbon (Battaglia Jr. et al., 2019), notably amino acids (AAs). However, the influence of AAs on iron redox chemistry and hydroxyl radical ($\bullet\text{OH}$) production in cloud water remains insufficiently understood.

Recent investigations have unveiled the presence of reactive oxygen species (ROS) in viscous aerosol particles, highlighting their pronounced reactivity in such environments (Alpert et al., 2021; Edwards et al., 2022). Hydroxy radicals ($\bullet\text{OH}$) emerge as primary ROS in the atmospheric water phase, with concentrations estimated between 10^{-14} to 10^{-12} M^{-1} (Bianco et al., 2020; Gligorovski et al., 2015). Key sources of $\bullet\text{OH}$ include gas-droplet partitioning and in situ formation through processes like photolysis at surfaces or in the bulk phase, such as the photolysis of TMI and hydrogen peroxide (H_2O_2) (Bianco et al., 2015; Tilgner et al., 2013).

Iron (Fe), copper (Cu), and manganese (Mn) have gained prominence as pivotal metals in atmospheric chemical processes due to their elevated concentrations, with Fe averaging around 10^{-6} M in the atmospheric aqueous phase (Sorooshian et al., 2013). Experimental evidence and

literature emphasize the crucial role of iron, particularly via (photo)-Fenton and (photo)-Fenton-like processes, in the generation and budgeting of $\bullet\text{OH}$ (R1-R5) (Guo et al., 2014; Tilgner et al., 2013).



While Fe(III)/Fe(II) ions precipitate as oxides or hydroxides at pH higher than 4.0, in the cloud water phase, iron complexes with organic ligands enhance stability under typical cloud water photooxidation conditions (Soriano-Molina et al., 2018; Yuan et al., 2020). Various organic ligands, including carboxylic acids and aldehydes, have been extensively studied (Long et al., 2013; Marion et al., 2018; Soriano-Molina et al., 2018). However, less than 30 % of the dissolved organic carbon (DOC) in the cloud-aqueous phase has been molecularly characterized, with AAs constituting a significant portion of DOC (Bianco et al., 2016). Numerous field studies have confirmed the presence of AAs in cloud water, rain, fog, and aerosols, with concentrations typically ranging from low nanomolar to micromolar levels, depending on the location and sampling method (Matos et al., 2016; van Pinxteren et al., 2023; Renard et al., 2022; Triesch et al., 2021). For example, Renard et al. (2022) detected more than 15 AAs in cloud water collected at Puy de Dôme, France, with glutamate being one of the most abundant species. These compounds originate from both primary emissions (e.g., bioaerosols, ocean spray) and secondary atmospheric processes (e.g., processing of proteins or peptides within clouds) (Mace et al., 2003; Samy et al., 2011). Amino acids, as key nitrogen-containing

components in organic matter, can significantly affect the oxidation capacity of cloud water through free radical scavenging and metal complexation reactions (Bianco et al., 2016; Marion et al., 2018), but their specific atmospheric reactivity and transformation mechanisms are still unclear. The photochemical behavior and fate of AAs in the atmosphere remain relatively unexplored. For example, tryptophan can undergo direct photolysis, producing low-molecular-weight compounds and dimerization products under solar-simulated conditions. Recent investigations into the fate of the Fe(III)-aspartate complex demonstrate ligand-to-metal charge transfer reactions (LMCT) and the formation of ammonia and short-chain carboxylic acids (Marion et al., 2018).

However, the effect of the complexation between Fe(II) and AAs on the rate of Fenton reaction and the yield of $\bullet\text{OH}$ in the atmosphere has not yet been investigated. Moreover, the effect of the complexation between Fe(III) and AAs on the quantum yield of atmospheric photolysis of Fe(III) deserves further investigation, since both processes highly affect the budget of $\bullet\text{OH}$ during the day and night in the atmosphere. In addition, the complexation between Fe(III) and AAs introduces two distinct photooxidation pathways: the photolysis of Fe-AAs complexes and reactions between AAs and (photo)-generated $\bullet\text{OH}$. Although both pathways significantly contribute to the transformation of AAs in cloud water and impact inorganic and organic chemical compositions, their mechanisms still lack further study, especially in terms of products generation.

This study specifically focuses on glutamic acid (Glu), an AAs regularly detected in cloud water and aerosols (van Pinxteren et al., 2012; Triesch et al., 2021), and on the investigation of its impact on iron (Fe(II)/Fe(III)) reactivity. The study explored i) the effect of Glu on the rate and $\bullet\text{OH}$ yield of the Fenton reaction; and ii) the effect of Glu on the $\bullet\text{OH}$ production and Fe(II)

quantum yield during the Fe(III) photolysis. In addition, the study explores iii) two pathways of Fe(III) and Fe(III)-Glu complex photolysis: the LMCT process and the reaction between Glu and $\bullet\text{OH}$, assessing their respective contributions to Glu fate. Utilizing competitive kinetic experiments, the contributions of each pathway were estimated, and a detailed investigation of the formation, and chemical mechanisms of transformation products was carried out. Ultimately, our study aims to quantify the diverse contributions of different pathways in amino acid conversion in the presence of iron.

2. MATERIAL AND METHODS

2.1. Chemicals

All chemicals were used without further purification: Fe(III)-perchlorate (99.9 %), Fe(II)-perchlorate (99.9 %), L-glutamic acid monosodium salt (Glu, 99 %), hydrogen peroxide (H_2O_2 , 30 %), malonic acid (99.0 %), and 2,4-dinitrophenylhydrazine (DNPH, 97 %) were purchased from Sigma Aldrich. Sodium formate (99.0 %), potassium oxalate monohydrate (99.0 %), sodium succinate dibasic (98.0 %), and 3-(2-pyridyl)-5,6-diphenyl-1,2,4-triazine-p, p'-sulfonic acid monosodium salt hydrate (Ferrozine, 97 %) were purchased from Fluka. Ammonium acetate (99.3 %) was purchased from Fisher. Water was purified using a reverse osmosis RIOS 5 and Synergy (Millipore) device (resistivity $18.2 \text{ M}\Omega \text{ cm}$, $\text{DOC} < 0.1 \text{ mg L}^{-1}$). All solutions were prepared in milli-Q water.

2.2. Experimental procedure

2.2.1. Fenton reaction

The Fenton experiments were carried out with Fe(II) perchlorate at room temperature and a pH of 5.6 ± 0.1 (Kinetic experiments) and 3.8 ± 0.1 (Electron spin resonance (ESR) experiments).

133 The pH of 5.6 was chosen to favor the formation of Fe(II)-Glu complexes during the kinetic
134 studies, while the lower pH of 3.8 was selected for ESR experiments, as $\bullet\text{OH}$ detection by ESR
135 is more effective under acidic conditions. These two pH values fall within the typical range
136 observed in atmospheric cloud water. Specifically, pH of 3.8 represents more acidic conditions
137 often found in polluted regions, whereas pH of 5.6 reflects the composition of cloud water in
138 remote or less impacted environments. This range enables the assessment of the system's
139 behavior under environmentally relevant conditions.

140 The Fenton kinetic experiments were initiated by the addition of the H_2O_2 stock solution. Hence,
141 the designed H_2O_2 concentration are 100 and 25 μM in kinetics and ESR experiment
142 respectively. The solution was continuously stirred during the reaction. The pH of the solution
143 was adjusted using HClO_4 or NaOH solutions. The samples were taken every 15 seconds and
144 mixed with a solution of Ferrozine in phosphate buffer ($\text{pH} = 7.0 \pm 0.1$) (Gabet et al., 2023).

145 Phenol was used as $\bullet\text{OH}$ scavenger in the experiment. As a scavenger, the required
146 concentration of phenol was calculated to quench $\bullet\text{OH}$ so that theoretically 99 % of $\bullet\text{OH}$ can be
147 trapped via reacting with phenol. The same method was used in the presence of Glutamic acid
148 (Glu) to study the Fe(II)-Glu complex Fenton-like reaction at the same pH. To get different
149 fractions of Fe(II)-Glu, Fe(II) was mixed with varying concentrations of Glu solution (0 - 25
150 mM) to calculate the reactivity constant of the Fenton reaction. The experimental data were
151 analyzed using Origin 2019 software. To determine and quantify the $\bullet\text{OH}$ generation in the
152 Fenton reaction, the ESR experiment was carried out using 5,5-dimethyl-1-pyrroline-N-oxide
153 (DMPO) as the spin trap. $\text{Fe}(\text{ClO}_4)_2$ and H_2O_2 were mixed with DMPO at a pH of 3.8 ± 0.1 .
154 The pH was set because the ESR signal intensity was lower at a higher $\text{pH} = 4.0$. ESR

spectroscopy was performed on a Bruker EMX-plus spectrometer using the resonator 4119HS. Detailed information was provided in the supplementary material section (SM1).

2.2.2. Photolysis of Fe(III)

To study the Fe(III) photolysis, isopropanol was used as a scavenger in the solution to quench the generated $\bullet\text{OH}$ radicals. The pH of the solution was adjusted to 3.8 ± 0.1 with HClO_4 or NaOH solutions. The Fe(III) solution was irradiated in a Pyrex jacketed cylindrical reactor (Fig. SM1) with a circulation cooling system to keep a constant temperature of 283 ± 0.2 K. The reactor was located at the focal point of a 500 W xenon lamp equipped with a Pyrex filter to remove wavelengths < 290 nm and a water filter for infrared radiation absorption. The solution was stirred with a Teflon-coated magnetic stirring bar to ensure homogeneity. The same setup was used for the photolysis experiments in the presence of Fe(III)-Glu complexes. Different fractions of Fe(III)-Glu were achieved by adding different amounts of a Glu 50 mM stock solution (designed $[\text{Glu}] = 0 - 200 \mu\text{M}$).

The emission spectrum of the irradiation setup was recorded using a calibrated CCD camera (Ocean Optics USB 2000+UV-Vis) coupled with an optical fiber. A total Energy of $8.38 \times 10^3 \mu\text{W cm}^{-2}$ was determined between 290 and 500 nm as shown in Fig. SM2. Compared to the natural solar emission spectrum, the UV region between 290 and 400 nm, which contribute for driving the photoreaction of Fe(III) and Fe(III)-Glu, shows a quite similar spectral profile, as reported in our previous publication (Bianco et al., 2015). The Energy and photonic flux (I_0) of the polychromatic irradiation at every nanometer wavelength are listed in Table SM1. Detailed information about the calculation of the Fe(III) and Fe(III)-Glu photolysis quantum yield is given in the supplementary material section (SM2). To quantify the $\bullet\text{OH}$ generation during the Fe(III) photolysis, isopropanol was used in excess (10 mM) as a selective $\bullet\text{OH}$ probe.

Isopropanol reacts with •OH to form acetone which was quantified by HPLC (see section 2.4) (Motohashi and Saito, 1993).

2.2.3. Photodegradation of Glu

To investigate the fate of Glu in various systems, experiments were performed using the previously described photoreactor setup. Glu solutions, either alone or mixed with Fe(III) and/or H₂O₂, were irradiated under simulated solar light at pH 3.8 ± 0.1. Samples were collected at specific time intervals and analyzed using HPLC-MS (see section 2.4). To calculate and compare the photodegradation kinetics of Glu in different systems, a pseudo-first-order kinetic model was applied, expressed as Equation (1):

$$-\ln(C_t/C_0) = k_{\text{obs}} t \quad \text{Eq (1)}$$

where C_0 represents the initial concentration of Glu, and C_t is the concentration of Glu at time t of irradiation. In addition, IC-MS and TOC analyses were performed to identify the generated by-products and assess the mineralization of Glu (see section 2.4).

2.3. Study of the speciation of the Fe(III)/Fe(II)-Glu complex

The speciation of the Fe(III)/Fe(II)-Glu complex was studied using the Hyss 2009 software. This analysis included the iron, iron-aqua, iron hydroxy, and iron-Glu complexes in the solution. The parameters used in the software, such as iron and Glu concentrations, kept consistent with the one in the experimental procedure. The stability constants (log K) used for the complexes, such as the Fe(II)-Glu and Fe(III)-Glu complexes, etc. are listed in **Table SM2**. These constants are derived from the Visual MINTEQ database or NIST database 46 and have been corrected for a temperature of 25 °C and an ionic strength (I) of 0 M. The detailed method is provided in the supplementary material section (**SM3**).

2.4. Chemical analysis

2.4.1. Fe(II), H₂O₂, and Acetone quantification

Iron (II) concentration was determined by using Ferrozine, which forms a stable magenta complex with Fe(II) (Fe(II)-ferrozine) (Gabet et al., 2023). Hydrogen peroxide concentration during experiments was determined by using a spectrofluorimetric quantification method (Bader et al., 1988). The concentration of generated acetone in the solution was evaluated by HPLC (Shimadzu NEXERA XR HPL) equipped with a photodiode array detector and an autosampler (Wang et al., 2005). **Fig. SM3** shows the calibration curve of Fe(II), H₂O₂, and acetone. More details are given in the supplementary material section (**SM4**).

2.4.2. UPLC-MS, IC-MS and TOC

The quantification of Glutamic acid (Glu) and the identification of its transformation products was conducted using a ThermoScientific Orbitrap Q-Exactive high-resolution mass spectrometry (HRMS) coupled with a ThermoScientific Ultimate 3000 RSLC ultra-high-performance liquid chromatography (UPLC) system. The quantification of carboxylic acid by-products and NH₄⁺ resulting from Glu degradation was performed using a Thermo-Fisher Scientific ICS-6000 Ionic chromatograph interfaced with a simple quadrupole mass spectrometer (ISQ-EC-Thermo Scientific). The total organic carbon (TOC) concentration in the aqueous solution was followed by a Shimadzu TOC 5050A analyzer. Detailed information is reported in the Supplementary Material section (**SM5**).

2.5. Kinetic Modeling

To verify the obtained experimental reactivity constants of the reaction between Fe(II)-Glu and H₂O₂, COPASI software was utilized to simulate the kinetics of Fe(II) consumption and

generation of $\bullet\text{OH}$ in the Fenton reaction in the presence of Glu using the default settings of the deterministic LSODA algorithm to solve ordinary differential equations (Hoops et al., 2006). The chemical reactions considered in the model are provided in **Table SM3**. The majority of rate constants used in the model were available in the literature or obtained from experimental results. For the unknown or uncertain rate constants, the value is obtained from the estimation according to a similar reaction.

3. RESULTS AND DISCUSSION

To investigate the effect of Glu on the Fe(II)/Fe(III) cycle, a complex set of experiments was performed. First, the complexation of Fe(II)/Fe(III) with Glu was studied as a function of pH and the initial concentration of Glu. Second, to study the effect of Glu on the Fenton reaction, its rate constants and $\bullet\text{OH}$ generation in the presence of Glu were obtained experimentally and using the kinetic model. The formation rates of Fe(II) and $\bullet\text{OH}$ were determined from Fe(III) photolysis with or without Glu. Finally, the mechanism of Glu photo-transformation was reported.

3.1. Complexation of Glu with Fe(II)/Fe(III)

The Fe speciation was initially investigated to understand how Glu interacts with iron ions under various conditions with Hyss2009 software. **Fig. SM4a** shows the speciation of 20 μM Fe(II) in the presence of Glu (0.2 – 25 mM) across a pH range of 4 to 10. It can be observed that Fe(II) predominates until pH = 5, while the fraction of the Fe(II)-Glu complex increases after this pH. Hence, a higher pH (5.6) was selected for the Fenton reaction to guarantee the presence of complex, while still working under aerosol/cloud conditions and to avoid iron precipitation occurring at higher pH values. At pH 5.6, the Fe(II)-Glu complex accounts for

2.2 % in the presence of 20 μM Fe(II) and 25 mM Glu. The complex fractions at varying Glu concentrations at pH = 5.6 are provided in **Table SM4**.

Fig. SM4b shows the simulated speciation of Fe(III) (100 μM) as a function of pH in the presence of Glu (10-20 μM). The Fe(III)-aqua, Fe(III)-hydroxy complexes, and Fe(III)-Glu complexes were observed as a function of the pH. At pH = 3.8, $[\text{Fe(III)}] = [\text{Glu}] = 100 \mu\text{M}$, the Fe(III)-hydroxy complexes Fe(OH)^{2+} and Fe(OH)_2^+ represent 24.4 and 22.8 % of the total Fe(III) concentration, respectively. In contrast, Fe(III)-Glu complex accounts for 52.3 % of the total Fe(III), while Fe(III)-aqua complex constitutes only 0.5 %. The UV-Vis spectra of Fe(III), Glu, and Fe(III)-Glu complex are depicted in **Fig. SM2**. The characteristic absorption band of Fe(III) with a maximum at 297 nm, corresponding to the charge transfer bands of Fe(OH)^{2+} , becomes attenuated in the presence of Glu. Moreover, the UV-Vis spectrum of Fe(III)-Glu mixture differs from those of Fe(III) and Glu alone or the simple overlap of their individual spectra, confirming the formation of a stable Fe(III)-Glu complex (Samavat et al., 2007). The fractions of the generated complex in the presence of different Glu concentrations at pH = 3.8 are given in **Table SM5**. For the sake of simplicity, Fe(III)/Fe(II)-hydroxy and Fe(III)/Fe(II)-aqua complexes are hereafter referred as Fe(III) and Fe(II).

3.2. Fenton reaction process in the presence of Glu

3.2.1. Fe(II) oxidation

To study the effect of Glu on the kinetics of the Fenton reaction and determine the rate constant of the reaction of Fe(II)-Glu with H_2O_2 , experiments were performed using different concentrations of Glu. **Fig. 1a** shows the faster Fe(II) concentration decreases when the Glu concentration increases, which indicates that Glu can increase the reaction rate of Fe(II) with H_2O_2 . This is likely due to the formation of the Fe(II)-Glu complex which has a high reaction

267 rate constant with H₂O₂. As seen in **Fig. 1b**, the data obtained by plotting $\frac{-\frac{d[\text{Fe(II)}]}{dt}}{[\text{H}_2\text{O}_2][\text{Fe(II)}]}$ as a
 268 function of the fraction of Fe(II)-Glu can be fitted with a linear equation $y = ax + b$, where a is
 269 equal to $1.54 \pm 0.13 \times 10^4 \text{ M}^{-1} \text{ s}^{-1}$ and represents the rate constant of reaction of Fe(II)-Glu with
 270 H₂O₂, and b is equal to rate constant of Fe(II) with H₂O₂ ($-\frac{d[\text{Fe(II)}]}{dt}$ data is provided in **Table.**
 271 **SM4**). Notably, obtained rate constant is significantly higher than the rate constant of the classic
 272 Fenton reaction which has a rate constant of about $50\text{-}70 \text{ M}^{-1} \text{ s}^{-1}$ (Kremer, 2003; Neyens and
 273 Baeyens, 2003; Rachmilovich-Calis et al., 2009). This results is very close to our recently
 274 published data as well, where the reactivity constant for the reaction between the FeC₂O₂ and
 275 H₂O₂ was determined to be $3.2 \pm 0.3 \times 10^3 \text{ M}^{-1} \text{ s}^{-1}$ (Scheres Firak, D. et al., 2025). This
 276 strongly indicates that the organic ligands highly enhance the reactivity of the iron with H₂O₂.
 277 The reason behind this increase is likely due to the Fe(II)-Glu complex accessing a lower
 278 reduction potential calculated to be $+ 0.241 \text{ V}$ compared with the Fe(II) ($+ 0.771 \text{ V}$)
 279 (Strathmann and Stone, 2002), which contributes to the higher rate constant of the reaction of
 280 Fe(II)-Glu with H₂O₂.
 281 Then the Fenton reaction model was used to fit the experimental data to verify the rate constant
 282 value of the reaction between Fe(II)-Glu and H₂O₂. As shown in **Fig. 1a**, the experimental data
 283 of Fe(II) kinetics can be well-fitted by the model. The fitted rate constant value of the reaction
 284 between Fe(II)-Glu and H₂O₂ was obtained at a range of 1.2×10^4 to $1.8 \times 10^4 \text{ M}^{-1} \text{ s}^{-1}$, which is
 285 very close to the experimental results.

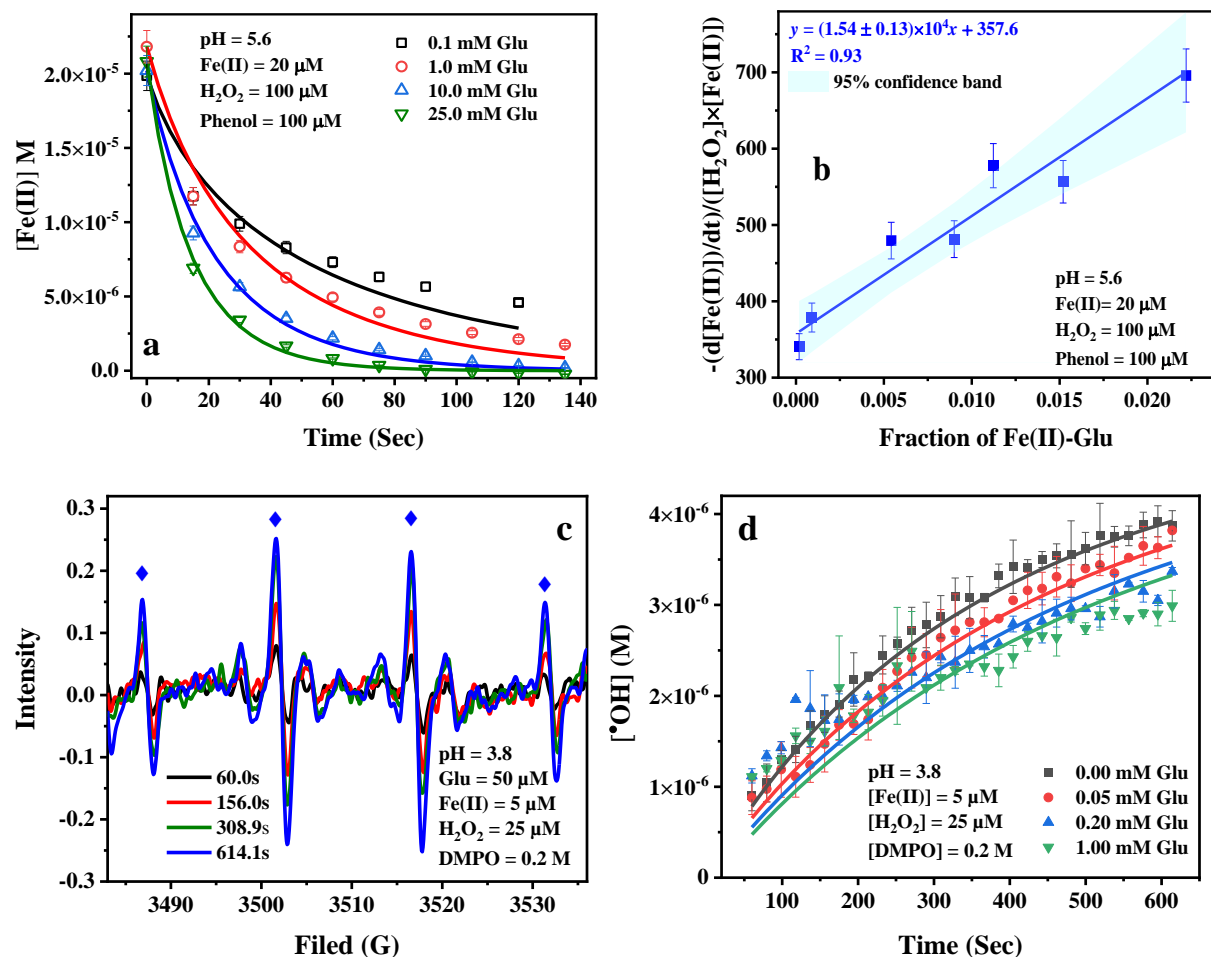


Fig. 1 Effect of different concentrations of Glu on the kinetics of Fenton reaction (a), apparent rate constant as a function of the fraction of Fe(II)-Glu (b), Signal of EPR corresponding to DMPO-OH (The symbol "◆" marks the position of the characteristic 1:2:2:1 EPR signal of the DMPO-OH adduct.) (c), the kinetics of •OH generation in Fenton reaction in the presence of different concentrations of Glu, (d). Points are determined experimentally, and lines in figures a and d are the fit of data using the kinetic model.

3.2.2. •OH quantification

To study the effect of Glu on the •OH generation, EPR experiments were carried out. **Fig. 1c** shows the EPR signal of DMPO-OH (1:2:2:1) increases with the reaction time, indicating that

•OH is continuously generated. In **Fig. 1d**, the concentration of generated •OH decreases when the Glu concentration increases from 0 to 1.0 mM. This trend suggests no direct •OH generation occurs from the reaction of Fe(II)-Glu with H₂O₂. This hypothesis has been verified by employing a kinetic model. The experimental data can be well fitted using the experimental rate constant $k_{\text{Fe(II)-Glu/H}_2\text{O}_2} = 1.54 \pm 0.13 \times 10^4 \text{ M}^{-1} \text{ s}^{-1}$.

3.3. Fe(III) photolysis in the presence of Glu

3.3.1. Fe(II) formation

To study the effect of Glu on the kinetics and determine the quantum yield of the photolysis of Fe(III), the photo-driven reaction was carried out in the presence of different concentrations of Glu (0-200 μM) under simulated solar light. **Fig. SM5a** shows that the Fe(II) generation rate decreases when the Glu concentration increases, which indicates that Glu slightly reduces the photoactivity of Fe(III). As shown in **Fig. 2a**, plotting the apparent quantum yield of Fe(II), $\Phi_{\text{Fe(II)}}^{\text{obs}}$, as a function of the fraction of Fe(III)-Glu complex, the quantum yield of Fe(II) decreases with the fraction of Fe(III)-Glu complex increasing. The linear fit can depict the kinetic data well with a regression coefficient equal to 0.99. As mentioned in **SM2**, the intercept represents the Fe(II) quantum yield of Fe(III) photolysis under polychromatic irradiation, which is equal to 0.216 ± 0.004 . This result is consistent with previous data (Bossmann et al., 1998). The slope represents the difference between Fe(II) quantum yield of the Fe(III) photolysis and the value of the photolysis of Fe(III)-Glu complex ($\Phi_{\text{Fe(III)-Glu}}^{\text{Fe(II)}} - \Phi_{\text{Fe(III)}}^{\text{Fe(II)}}$), which is equal to -0.179, hence the Fe(II) quantum yield during the photolysis of Fe(III)-Glu is calculated to be 0.037 ± 0.004 . Weller et al. (Weller et al., 2013) investigated the photolysis of Fe(III)-carboxylate complexes and found the quantum yield of Fe(II) formation from Fe(III)-malonate

at 308 nm and 351 nm, with values of 0.024 ± 0.001 and 0.040 ± 0.003 respectively. This suggests that Fe(III) complexes containing unsubstituted carboxylates as a functional group exhibit lower quantum yields compared to Fe(III).

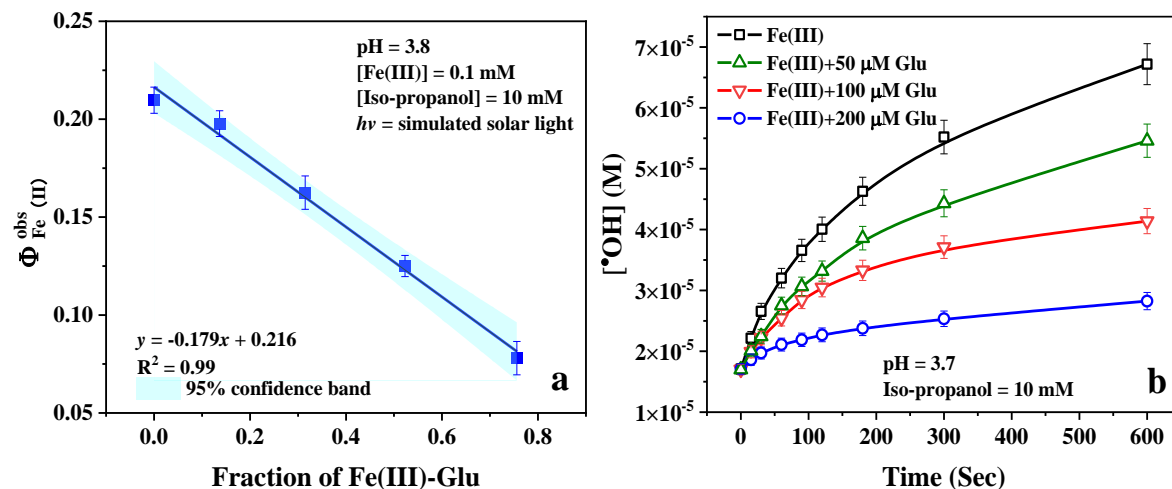


Fig. 2 a) The quantum yield of Fe(III) photolysis as a function of the fraction of Fe(III)-Glu complex; b) The $^{\bullet}OH$ generation of Fe(III) photolysis in the presence of different concentrations of Glu. The continuous lines are visual guides generated by applying the "Connect B-Spline" function in Origin 2019.

3.3.2. $^{\bullet}OH$ generation

Since the photolysis of Fe(III) is an important process affecting the budget of $^{\bullet}OH$ in the atmosphere (Guo et al., 2014), the effect of Glu on the $^{\bullet}OH$ produced by the photolysis process of Fe(III) was investigated. As shown in **Fig. SM5b**, the acetone generation rate decreases when the Glu concentration increases, indicating that the $^{\bullet}OH$ generation of the Fe(III) photolysis decreases in the presence of Glu (**Fig. 2b**). The most likely reason for this observation is the decrease of the Fe(III) hydroxy complexes (**Table SM5**), hence the decrease of the $^{\bullet}OH$ yield as the Fe(III)-Glu does not produce $^{\bullet}OH$ directly, but instead forms Glu oxidation products

(Glu_{ox}) through the LMCT process. These Glu oxidation products can complex Fe(II) and regenerate Fe(III), a mechanism known as “the quenching mechanism” proposed by Wang et al (2010)(Wang et al., 2010). This process reduces the apparent quantum yield of Fe(II) to 0.037 ± 0.004 . This result illustrates that •OH generation could be less in the presence of amino acids during the daytime in the atmosphere.

3.4. The Glu fate in the presence of Fe(III) under simulated solar light

3.4.1 Photodegradation of Glutamic acid in different systems

All the above results indicate that Glu not only stabilizes Fe(III)/Fe(II) at higher pH but also influences the Fenton reaction and photolysis of Fe(III) processes. The main effects were that the complexes altered the individual reaction rate constants and •OH production. On the other hand, Glu as the organic ligand can also be degraded during the reaction, especially photo-reaction in the atmosphere. **Fig. 3** shows the photodegradation kinetics of Glu in different systems, and the first-order fitted data is reported in **Fig. SM6**. As expected, when only Glu was present in the solution, no significant degradation ($k_{\text{obs}} = 1.90 \pm 0.22 \times 10^{-5} \text{ s}^{-1}$) was observed after 1 hour of irradiation, as shown in the UV-Vis spectrum (**Fig. SM2**) of Glu, since there is no significant absorption of solar radiation. The Glu degradation efficiency slightly increased in the presence of 1 mM H₂O₂ with a degradation constant of $2.44 \pm 0.45 \times 10^{-5} \text{ s}^{-1}$ corresponding with a degradation of 8.5 % in 1 hour, which is due to the formation of •OH radicals via the photolysis of H₂O₂. In addition, the rate constant of •OH with Glu is $2.3 \times 10^8 \text{ M}^{-1} \text{ s}^{-1}$ (Masuda et al., 1973), which means that the reaction between those two components is one of the most important processes for the degradation of Glu. Considering the second reaction rate constant between •OH and H₂O₂ ($k_{\text{H}_2\text{O}_2}^{\text{•OH}} = 2.7 \times 10^7 \text{ M}^{-1} \text{ s}^{-1}$) (Christensen et al., 1982), it can be argued

that under adopted conditions, about 55 % of generated $\bullet\text{OH}$ was quenched by the H_2O_2 , which led to the formation of less reactive hydroperoxyl radical/superoxide anion pair ($\text{HO}_2\bullet/\text{O}_2^{\bullet-}$).

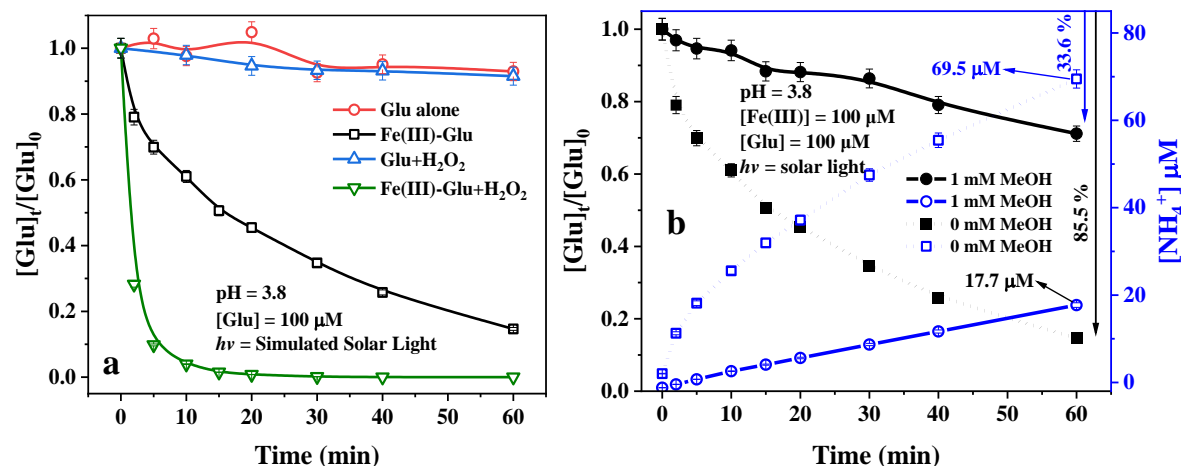


Fig. 3 a) Photodegradation of Glu in different systems: Glu alone, Fe(III)-Glu; Glu+ H_2O_2 and Fe(III)-Glu+ H_2O_2 ($[\text{Glu}] = 100 \mu\text{M}$, $[\text{Fe(III)}] = 100 \mu\text{M}$, $[\text{H}_2\text{O}_2] = 1 \text{ mM}$). b) Photodegradation of Glu and ammonium generation in the Fe(III)-Glu system in the absence and presence of MeOH. The continuous lines are visual guides generated by applying the "Connect B-Spline" function in Origin 2019.

Moreover, in the presence of Fe(III), the mixture of Fe(III)-hydroxy and Fe(III)-Glu complexes underwent the photolysis process. As shown in **Fig. 3a**, about 85 % of Glu was degraded with a first-order rate constant of $4.99 \pm 0.24 \times 10^{-4} \text{ s}^{-1}$ after 1 hour of irradiation. This high efficiency is likely due to two different Glu degradation pathways, one is due to the reaction between Glu and the $\bullet\text{OH}$ radicals generated by photolysis of Fe(III) (R1 and R2), and the other one is due to the direct photolysis of Fe(III)-Glu leading to the formation of Fe(II) and oxidation products of the organic ligand (Glu_{ox}). The synergistic effect of those two processes highly improved the Glu degradation efficiency. To distinguish between the contributions of the two degradation pathways, methanol was selected as $\bullet\text{OH}$ scavenger ($k_{\text{Methanol}}^{\bullet\text{OH}} = 9.7 \times 10^8 \text{ M}^{-1} \text{ s}^{-1}$) (Buxton et al.,

1988). As illustrated in **Fig. 3b**, Glu degradation was inhibited by 60 %, indicating that 40 % of Glu degradation originates from the photolysis of Fe(III)-Glu complexes. Interestingly, this ratio aligns with the proportion of Fe(III) and Fe(III)-Glu complexes in the system (**Table SM5**), confirming the aforementioned conclusion. Furthermore, the degradation of Glu resulting from the photolysis of Fe(III)-Glu complexes likely does not involve a $\bullet\text{OH}$ process (Sun et al., 1998; Weller et al., 2013).

Glu degradation was observed to be approximately 100 % after 20 mins of irradiation in the presence of Fe(III) and H_2O_2 , with a first-order rate constant of $5.13 \pm 1.03 \times 10^{-3} \text{ s}^{-1}$. Compared to conditions with only Fe(III) or H_2O_2 , the efficiency of Glu degradation significantly improves due to the photo-Fenton reaction in the system, which greatly accelerates the formation rate of reactive species and consequently enhances the degradation rate of Glu.

3.4.2. Analysis of photodegradation products of glutamic acid

To distinguish the Glu degradation processes resulting from the photolysis of Fe(III)-Glu complexes and from those caused by $\bullet\text{OH}$ attack, which might lead to the formation of different products, a series of experiments were conducted. In all cases, IC-MS was employed to analyze the formation of short-chain carboxylic acid and ammonium ions, providing a deeper understanding of the photochemical reaction products in various systems under simulated solar light.

Figure 4a depicts the formation of ammonium (NH_4^+) in different systems under irradiation. A positive correlation is observed between the rate of NH_4^+ production and the rate of Glu degradation in various systems, suggesting the occurrence of deamination during the Glu degradation. Additionally, several carboxylic acids (i.e. acetic, formic, succinic, malonic, and

oxalic acids) were detected (**Table SM6**), as illustrated in **Fig. 4b**, **4c**, and **4d**. Notably, the concentration of generated carboxyl acids is considerably lower than that of NH_4^+ .

After 120 min of irradiation, low concentrations of generated NH_4^+ and carboxylic acid were determined during Glu photolysis due to small Glu degradation (see **Fig. 4a** and **Fig. SM7**). In the presence of 1 mM H_2O_2 , NH_4^+ concentration increased to 7.8 μM within 120 min, representing a 3-fold increase compared to that produced during Glu photolysis. **Fig. 4b** demonstrates the formation of carboxylic acids with formate and succinate as primary carboxylate products, while a negligible concentration of acetate (less than 1 μM) was also detected, all of which are products of $\bullet\text{OH}$ attack.

In the presence of Fe(III), NH_4^+ concentration increased to 69.5 μM (**Fig. 4a**) within 60 min. Simultaneously, the generation of carboxyl acids, such as formate, acetate, and oxalate was observed. The concentration of formate initially increased, reaching a plateau value of 8.7 μM at 20 min, after decreasing to approximately 6.4 μM at 60 min. The reason for the decline is probably the reaction to photo-generated $\bullet\text{OH}$ ($k_{\text{Formate}}^{\bullet\text{OH}} = 1.3\text{--}1.4 \times 10^8$) (Buxton et al., 1988).

Acetate concentration increased throughout the reaction, reaching 10.9 μM at 60 min. Other carboxylates, such as succinate, malonate, and oxalate, were found in lower concentration, with a maximum of around 2 μM within 5 min. As mentioned above, in the presence of Fe(III), the Glu degradation can be attributed to two pathways: one resulting from $\bullet\text{OH}$ attack, on the other from the photolysis of the Fe(III)-Glu complexes.

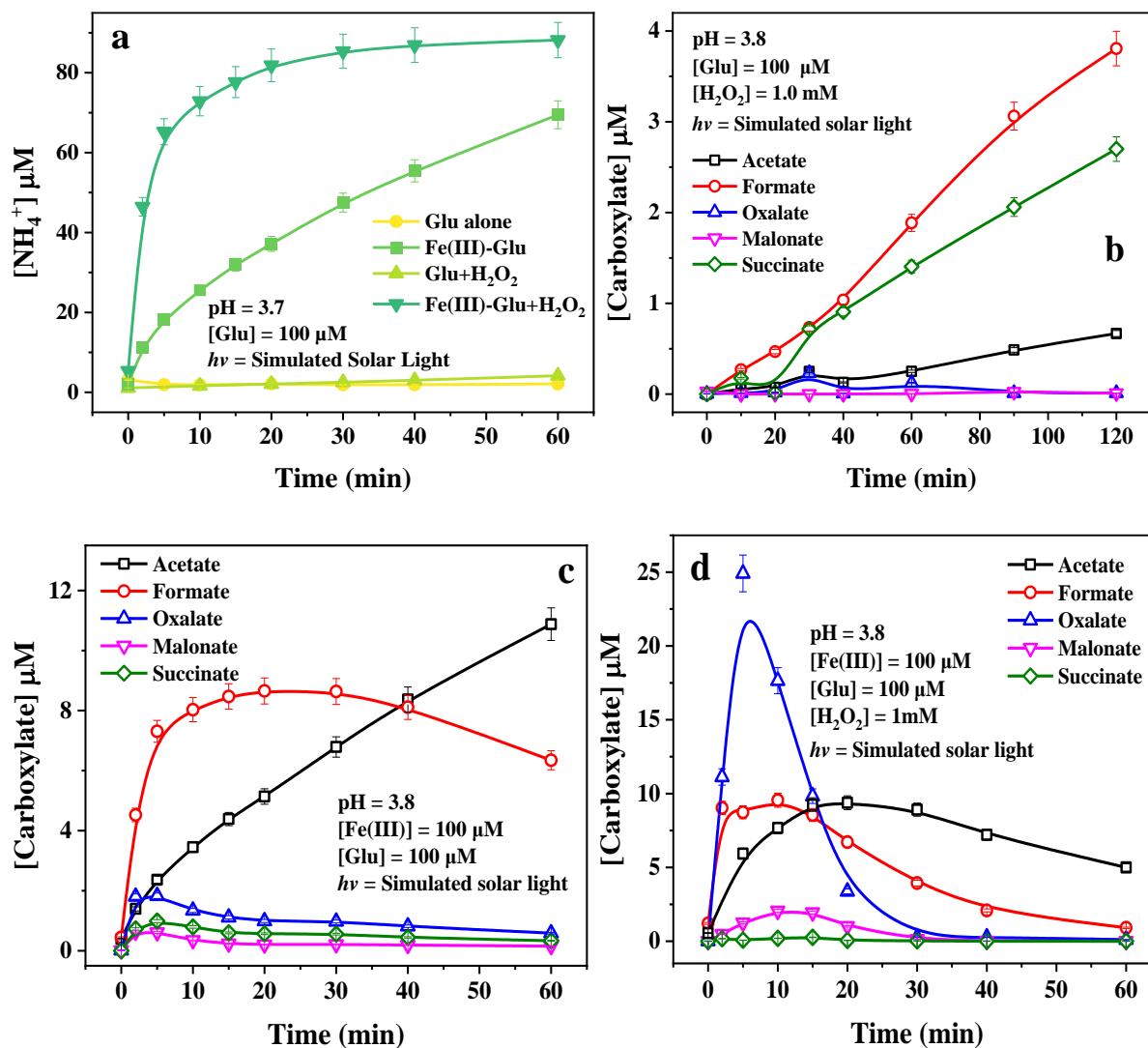


Fig. 4. The by-products of Glu degradation under solar light a) formation of NH_4^+ in different systems; formation of carboxylic acids b) in the system $\text{Glu}+\text{H}_2\text{O}_2$; c) in the system $\text{Glu}+\text{Fe(III)}$ and d) in the system $\text{Glu}+\text{Fe(III)}+\text{H}_2\text{O}_2$. The continuous lines are visual guides generated by applying the "Connect B-Spline" function in Origin 2019.

To distinguish the contribution of these two pathways, isopropanol was employed to quench $\cdot\text{OH}$ in solution generating acetone as the main product (Motohashi and Saito, 1993). As shown in **Fig. SM8**, only acetate and formate were generated (succinate, malonate, and oxalate were not detected). Moreover, the presence of isopropanol significantly enhanced the formation of

acetate compared to values observed with only Fe(III) and Glu. This is likely due to the H-donor effect of the added alcohol or to the reaction between acetic acid radicals (HOOCCH_2^\bullet) and HO_2^\bullet radicals, the latter being generated through the reaction of $^\bullet\text{OH}$ with the alcohol. As shown in **Fig. SM8**, the concentration of generated formate in the presence of isopropanol and Fe(III) is lower than that when only Fe(III) is added, suggesting that formate was likely not a primary product generated from the photolysis of Fe(III)-Glu complexes but rather may be produced by $^\bullet\text{OH}$ attack of other carboxylic acids. For example, the generated acetate can be further oxidized reacting with $^\bullet\text{OH}$ leading to the formation of formate.

This finding is consistent with the result observed in the presence of H_2O_2 alone (**Fig. SM7**). In the presence of $^\bullet\text{OH}$ scavenger, the generation of NH_4^+ was strongly inhibited with the formation of 17.7 μM instead of 69.5 μM after 1 h (as previously reported in **Fig. 3b**), which indicates that the NH_4^+ formation is mainly due to the $^\bullet\text{OH}$ attack process. Furthermore, a significant NH_4^+ (up to 69.5 μM within 60 min) can be observed in the presence of both Fe(III) and H_2O_2 (**Fig.4d**). Oxalate, acetate, and formate were observed as the predominant carboxylate products with higher concentrations, reaching 24.9, 9.4, and 9.6 μM respectively, before decreasing. Additionally, the formations of malonate (2.1 μM) and succinate (0.3 μM) were observed at lower concentrations during the photoreaction. In the presence of H_2O_2 and Fe(III), the Fe(III)/Fe(II)-cycle is enhanced via the photo-Fenton reaction. Fe(II) is rapidly re-oxidized to Fe(III) to produce $^\bullet\text{OH}$, which then directly attacks Glu, leading to degradation. Fe(III) is re-complexed by Glu reactivating the photoreaction and then the iron cycle. Therefore, the addition of H_2O_2 favors deamination as well as various carbon-centered radical combination interactions. The rapid depletion of oxalate after 30 min implies that photolysis of complexes between Fe(III) and polycarboxylic acid also occurs in this system, while formate, acetate, and

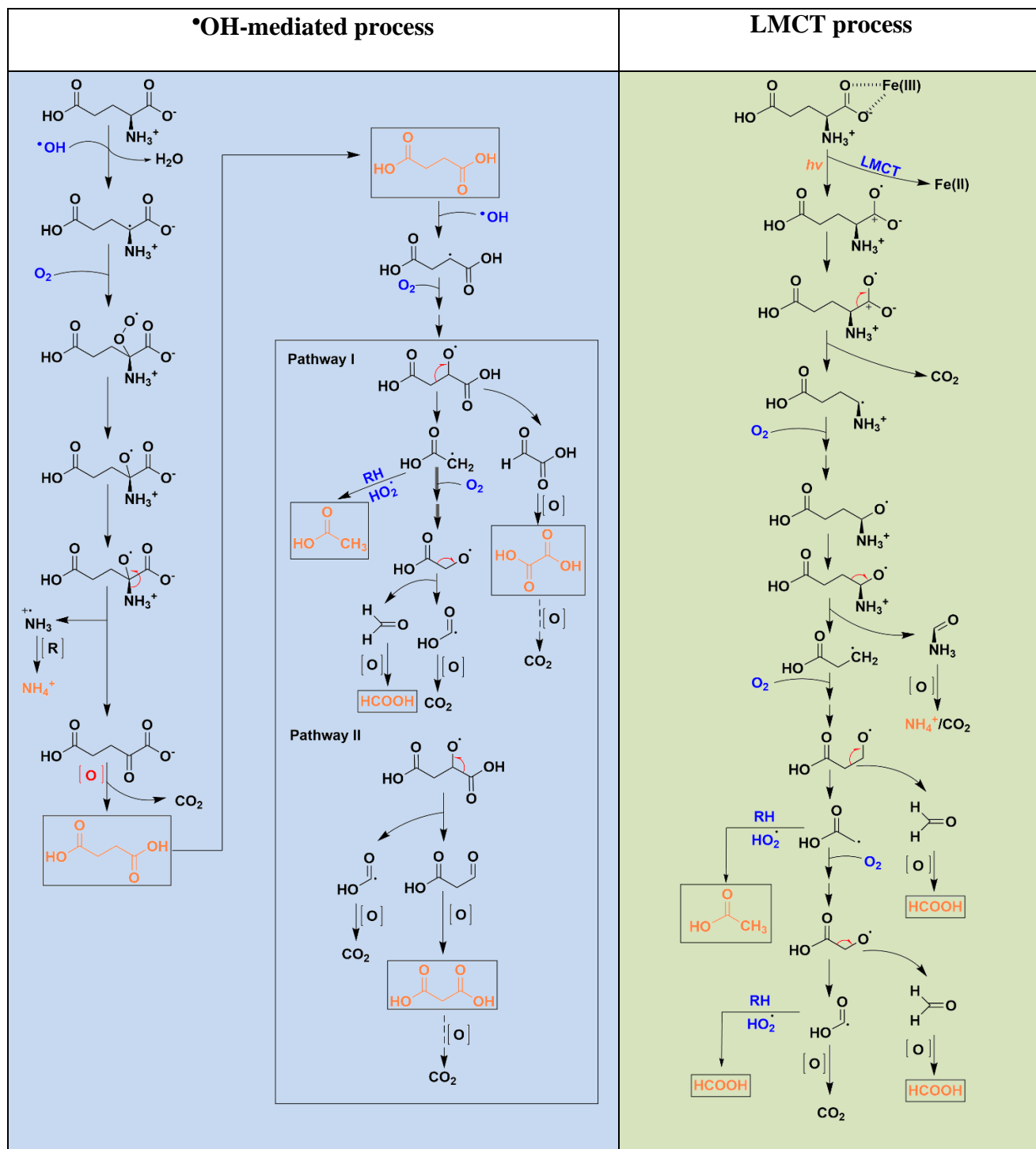
malonate exhibit similar tendencies with different reaction rates. To verify the mineralization of Glu during the reaction, a TOC was followed during the reaction. As shown in **Fig. SM9a**, the mineralization efficiency of Glu in the presence of Fe(III) and H₂O₂ is significantly higher than that observed when only Fe(III) is present, due to the presence of the photo-Fenton process. This finding is consistent with the degradation efficiency of Glu presented in **Figure 3a**. Hence, these results illustrate that Glu was mineralized to form CO₂ and H₂O. Moreover, the TOC values obtained experimentally are higher than the values calculated from the concentration of Glu and carboxylic acid products, indicating the presence of other organic compounds in the system. Along these organic substances cannot be detected under our experimental conditions, they will enter the cloud water gas phase, further participating in atmospheric photochemical reactions and eventually being mineralized into H₂O and CO₂. In the presence of H₂O₂, as Glu undergoes photodegradation, the concentration of H₂O₂ in the system continues to decrease until it is completely consumed (**Fig. SM9b**).

3.5. Insight into the mechanism of Glu transformation

The light-driven transformation mechanism of Glu in the presence of Fe(III) was investigated, with a focus on the [•]OH-mediated and the ligand-to-metal charge transfer (LMCT) process. The key difference between the two processes lies in the generation of glutamate radicals: the [•]OH-mediated process involves a free radical mechanism initiated by hydrogen abstraction, whereas the LMCT pathway proceeds via an electron transfer process driven by photoexcitation. To provide a clear comparison, the two mechanisms are illustrated separately in **Scheme. 1** summarizing the possible Glu degradation pathway, derived from IC-MS analysis of the detected products.

In the $\bullet\text{OH}$ -mediated process, the α - carbon of Glu is identified as the primary site attacked for $\bullet\text{OH}$ attack, initiating the transformation process. Hydrogen abstraction by $\bullet\text{OH}$ results in the formation of glutamate alkyl radical ($\text{R-C}^\bullet(\text{COO}^-)\text{NH}_3^+$) and H_2O . Subsequently, this alkyl radical reacts with O_2 to generate the alkylperoxy radical (ROO^\bullet), which is further converted to alkoxy radical (RO^\bullet) (Goldman et al., 2021; von Sonntag and Schuchmann, 1991). The formation of RO^\bullet is followed by a deamination process, which leads to the formation of ammonium (NH_4^+) and 2-oxoadipic acid through the cleavage of the amino group (Vel Leitner et al., 2002). Due to the presence of an oxo group ($\text{C}=\text{O}$) adjacent to a carboxyl group (COOH), 2-oxoadipic acid is chemically unstable and prone to self-decomposition via decarboxylation, resulting in the formation of succinic acid (Penteado et al., 2019). Further oxidation of succinic acid produces smaller carboxylic acids.

In contrast, the LMCT process is initiated upon irradiation, resulting in the reduction of Fe(III) to Fe(II) and the generation of a radical centered on the oxygen atom of α -carboxyl group of glutamic acid ($\text{R-CH}(\text{NH}_3^+)\text{C}^+\text{O}^\bullet\text{O}^-$). This high reactive radical undergoes a decarboxylation process resulting in the formation of an alkyl radical ($\text{R-CH}^\bullet\text{NH}_3^+$). Subsequently, the radical chain reaction propagates in the presence of O_2 , leading to the formation of smaller carboxylic acids. It is critical to highlight that the only carboxylic acids detected under the same conditions are formic acid and acetic acid. This is different from the $\bullet\text{OH}$ -mediated process, in which succinate is first formed and then further decomposed into compounds such as other small molecular carboxylic acids.



492 **Scheme 1.** The mechanism of Glu degradation in the presence of Fe(III): by $\bullet\text{OH}$ attacking
 493 process and LMCT process. Products in orange are detected by IC-MS.

494

4. ATMOSPHERIC IMPLICATION

This study systematically investigated the complexation of Glu with Fe(II)/Fe(III), its effect on the typical atmospheric reactions (Fenton reaction and Fe(III) photolysis), and its fate in the atmospheric aqueous phase. Our findings reveal that iron-amino acid complexes (Fe-AAs) significantly modify the Fe(II)/Fe(III) cycle and $\bullet\text{OH}$ budget, diverging from the "classic" photo-Fenton mechanisms. Specifically, Fe(II)-Glu reacts with H_2O_2 at a rate constant two orders of magnitude higher than Fe(II) alone, potentially improving the iron cycle. Conversely, Fe(III)-Glu exhibits a lower quantum yield under irradiation, suppressing the Fe(III)/Fe(II) cycle. Moreover, both reactions result in lower $\bullet\text{OH}$ generation, as they favor the formation of Glu oxidation products (Glu_{ox}), thus partially affecting atmospheric oxidative capacity.

To date, the concentration of the Fe(II)/Fe(III)-Glu in cloud water has not yet been directly measured. Hence, based on the reported mean concentrations of Glu (87 nM) (Renard et al., 2022), Fe(II) (1 μM) (Deguillaume et al., 2014), and Fe(III) (0.5 μM) (Deguillaume et al., 2014) in cloud water from the Puy de Dôme station (PUY - France), the fraction of Fe(II)-Glu and Fe(III)-Glu was calculated to be around 8.7×10^{-10} - 2.1×10^{-4} % and 6.1×10^{-2} - 2.4×10^{-1} % using Hyss software at a pH range of 3 - 7, respectively. Cloud water span a wide pH range (3–7), which influences iron speciation and redox cycling. Low pH enhances iron solubility but may reduce Fe–Glu complexation by altering ligand binding. Nevertheless, in polluted regions with elevated iron and amino acid levels, the absolute Fe–Glu concentration may remain appreciable despite a lower complexation fraction. In contrast, marine clouds often contain lower concentrations of both Fe and amino acid (like Glu is around 33 pM collected in Venice on the Sacca San Biagio Island (Barbaro et al., 2011)), leading to a smaller Fe-Glu fraction. Moreover, the concentration of Glu in cloud droplets may increase during the cloud water evaporation,

leading to an increase in the proportion of iron-Glu complexes. This shift could alter atmospheric Fenton reaction dynamics, reducing $\bullet\text{OH}$ production, particularly at night (Galloway et al., 2014; Shulman et al., 1997). Similarly, the lower quantum yield of the Fe(III)-Glu under irradiation inhibits the Fe(II)/Fe(III) cycle and $\bullet\text{OH}$ generation especially in daytime conditions. Likewise, the variations in light intensity due to diurnal cycles and cloud cover modulate the photolysis rates of iron–ligand complexes and the generation of reactive radicals. Taken together, these factors suggest that the efficiency and pathways of the observed processes are highly dynamic in atmospheric aqueous phases, underscoring the need to incorporate these dependencies into atmospheric models.”

In addition, recent studies reported that the average AAs contribution corresponded to 9.1 % of the dissolved organic carbon (DOC) (Bianco et al., 2016), highlighting their significance. Hence, Fe-AAs play a crucial role in iron speciation, stability, and $\bullet\text{OH}$ budget in atmospheric aqueous phases, which suggests that the inclusion of Fe-AAs in atmospheric aqueous phase models is essential for accurately estimating $\bullet\text{OH}$ production, a key driver of atmospheric oxidation. Moreover, irradiation of Glu in the presence of Fe(III), demonstrated two different mechanisms ($\bullet\text{OH}$ mediated and LMCT process) leading to the generation of different products, which can further influence the atmospheric chemical composition, particularly through the formation of aqueous secondary organic aerosols (aqSOA) (Ervens et al., 2014). Overall, the generation of NH_4^+ is regarded as a link between organic nitrogen species and inorganic nitrogen in cloud water. The generation of carboxylic acids further increases atmospheric complexity, as the generated carboxylic acids (e.g., oxalic acid) can be complex with iron and participate in the consequent photoreactions. In fact, atmospheric models often simplify the distribution and interactions of transition metal ions (TMIs) with organic compounds, including AAs. This study

highlights the crucial role of the LMCT process in AAs oxidation, which should be considered in atmospheric modeling as well.

ACKNOWLEDGMENT

This work was supported by the Agence Nationale de la Recherche of France in the frame of the PRCI project REACTE.

AUTHOR CONTRIBUTION

Peng Cheng: Investigation, Formal analysis, Writing – original draft; **Gilles Mailhot:** Funding acquisition, Review & editing, Supervision; **Mohamed Sarakha:** Review & editing, Supervision, **Guillaume Voyard:** Technical support; **Daniele Scheres Firak, Thomas Schaefer, Hartmut Herrmann:** Review & editing; **Marcello Brigante:** Conceptualization, Writing-review & editing, Supervision.

REFERENCE

- Alpert, P. A., Dou, J., Corral Arroyo, P., Schneider, F., Xto, J., Luo, B., Peter, T., Huthwelker, T., Borca, C. N., Henzler, K. D., Schaefer, T., Herrmann, H., Raabe, J., Watts, B., Krieger, U. K., and Ammann, M.: Photolytic radical persistence due to anoxia in viscous aerosol particles, *Nature Communications*, 12, 1769, <https://doi.org/10.1038/s41467-021-21913-x>, 2021.
- Angle, K. J., Neal, E. E., and Grassian, V. H.: Enhanced Rates of Transition-Metal-Ion-Catalyzed Oxidation of S(IV) in Aqueous Aerosols: Insights into Sulfate Aerosol Formation in the Atmosphere, *Environmental Science & Technology*, 55, 10291–10299, <https://doi.org/10.1021/acs.est.1c01932>, 2021.
- Bader, H., Sturzenegger, V., and Hoigné, J.: Photometric method for the determination of low concentrations of hydrogen peroxide by the peroxidase catalyzed oxidation of N,N-diethyl-*p*-phenylenediamine (DPD), *Water Research*, 22, 1109–1115, [https://doi.org/10.1016/0043-1354\(88\)90005-X](https://doi.org/10.1016/0043-1354(88)90005-X), 1988.

Barbaro, E., Zangrando, R., Moret, I., Barbante, C., Cescon, P., and Gambaro, A.: Free amino acids in atmospheric particulate matter of Venice, Italy, *Atmospheric Environment*, 45, 5050–5057, <https://doi.org/10.1016/j.atmosenv.2011.01.068>, 2011.

Battaglia Jr., M. A., Weber, R. J., Nenes, A., and Hennigan, C. J.: Effects of water-soluble organic carbon on aerosol pH, *Atmospheric Chemistry and Physics*, 19, 14607–14620, <https://doi.org/10.5194/acp-19-14607-2019>, 2019.

Bianco, A., Passananti, M., Perroux, H., Voyard, G., Mouchel-Vallon, C., Chaumerliac, N., Mailhot, G., Deguillaume, L., and Brigante, M.: A better understanding of hydroxyl radical photochemical sources in cloud waters collected at the puy de Dôme station – experimental versus modelled formation rates, *Atmospheric Chemistry and Physics*, 15, 9191–9202, <https://doi.org/10.5194/acp-15-9191-2015>, 2015.

Bianco, A., Voyard, G., Deguillaume, L., Mailhot, G., and Brigante, M.: Improving the characterization of dissolved organic carbon in cloud water: Amino acids and their impact on the oxidant capacity, *Scientific Reports*, 6, 37420, <https://doi.org/10.1038/srep37420>, 2016.

Bianco, A., Vaïtilingom, M., Bridoux, M., Chaumerliac, N., Pichon, J.-M., Piro, J.-L., and Deguillaume, L.: Trace Metals in Cloud Water Sampled at the Puy De Dôme Station, *Atmosphere*, 8, 225, <https://doi.org/10.3390/atmos8110225>, 2017.

Bianco, A., Deguillaume, L., Vaïtilingom, M., Nicol, E., Baray, J.-L., Chaumerliac, N., and Bridoux, M.: Molecular Characterization of Cloud Water Samples Collected at the Puy de Dôme (France) by Fourier Transform Ion Cyclotron Resonance Mass Spectrometry, *Environmental Science & Technology*, 52, 10275–10285, <https://doi.org/10.1021/acs.est.8b01964>, 2018.

Bianco, A., Passananti, M., Brigante, M., and Mailhot, G.: Photochemistry of the Cloud Aqueous Phase: A Review, *Molecules*, 25, 423, <https://doi.org/10.3390/molecules25020423>, 2020.

Bossmann, S. H., Oliveros, E., Göb, S., Siegwart, S., Dahlen, E. P., Payawan, L., Straub, M., Wörner, M., and Braun, A. M.: New Evidence against Hydroxyl Radicals as Reactive Intermediates in the Thermal and Photochemically Enhanced Fenton Reactions, *The Journal of Physical Chemistry A*, 102, 5542–5550, <https://doi.org/10.1021/jp980129j>, 1998.

Buxton, G. V., Greenstock, C. L., Helman, W. P., and Ross, A. B.: Critical Review of rate constants for reactions of hydrated electrons, hydrogen atoms and hydroxyl radicals ($\cdot\text{OH}/\text{O}-$

596 in Aqueous Solution, *Journal of Physical and Chemical Reference Data*, 17, 513–886,
 597 <https://doi.org/10.1063/1.555805>, 1988.

598 Christensen, H., Sehested, K., and Corfitzen, H.: Reactions of hydroxyl radicals with hydrogen
 599 peroxide at ambient and elevated temperatures, *The Journal of Physical Chemistry*, 86, 1588–
 600 1590, <https://doi.org/10.1021/j100206a023>, 1982.

601 Deguillaume, L., Charbouillot, T., Joly, M., Vaïtilingom, M., Parazols, M., Marinoni, A.,
 602 Amato, P., Delort, A.-M., Vinatier, V., Flossmann, A., Chaumerliac, N., Pichon, J. M., Houdier,
 603 S., Laj, P., Sellegri, K., Colomb, A., Brigante, M., and Mailhot, G.: Classification of clouds
 604 sampled at the puy de Dôme (France) based on 10 yr of monitoring of their physicochemical
 605 properties, *Atmospheric Chemistry and Physics*, 14, 1485–1506, [https://doi.org/10.5194/acp-](https://doi.org/10.5194/acp-14-1485-2014)
 606 14-1485-2014, 2014.

607 Edwards, K. C., Klodt, A. L., Galeazzo, T., Schervish, M., Wei, J., Fang, T., Donahue, N. M.,
 608 Aumont, B., Nizkorodov, S. A., and Shiraiwa, M.: Effects of Nitrogen Oxides on the Production
 609 of Reactive Oxygen Species and Environmentally Persistent Free Radicals from α -Pinene and
 610 Naphthalene Secondary Organic Aerosols, *The Journal of Physical Chemistry A*, 126, 7361–
 611 7372, <https://doi.org/10.1021/acs.jpca.2c05532>, 2022.

612 Ervens, B., Sorooshian, A., Lim, Y. B., and Turpin, B. J.: Key parameters controlling OH-
 613 initiated formation of secondary organic aerosol in the aqueous phase (aqSOA), *Journal of*
 614 *Geophysical Research: Atmospheres*, 119, 3997–4016, <https://doi.org/10.1002/2013JD021021>,
 615 2014.

616 Gabet, A., Guy, C., Fazli, A., Métivier, H., de Brauer, C., Brigante, M., and Mailhot, G.: The
 617 ability of recycled magnetite nanoparticles to degrade carbamazepine in water through photo-
 618 Fenton oxidation at neutral pH, *Separation and Purification Technology*, 317, 123877,
 619 <https://doi.org/10.1016/j.seppur.2023.123877>, 2023.

620 Galloway, M. M., Powelson, M. H., Sedehi, N., Wood, S. E., Millage, K. D., Kononenko, J. A.,
 621 Rynaski, A. D., and De Haan, D. O.: Secondary Organic Aerosol Formation during Evaporation
 622 of Droplets Containing Atmospheric Aldehydes, Amines, and Ammonium Sulfate,
 623 *Environmental Science & Technology*, 48, 14417–14425, <https://doi.org/10.1021/es5044479>,
 624 2014.

625 Gligorovski, S., Strekowski, R., Barbati, S., and Vione, D.: Environmental Implications of
 626 Hydroxyl Radicals (\bullet OH), *Chemical Reviews*, 115, 13051–13092,
 627 <https://doi.org/10.1021/cr500310b>, 2015.

628 Goldman, M. J., Green, W. H., and Kroll, J. H.: Chemistry of Simple Organic Peroxy Radicals
 629 under Atmospheric through Combustion Conditions: Role of Temperature, Pressure, and NO_x
 630 Level, *The Journal of Physical Chemistry A*, 125, 10303–10314,
 631 <https://doi.org/10.1021/acs.jpca.1c07203>, 2021.

632 Guo, J., Tilgner, A., Yeung, C., Wang, Z., Louie, P. K. K., Luk, C. W. Y., Xu, Z., Yuan, C.,
 633 Gao, Y., Poon, S., Herrmann, H., Lee, S., Lam, K. S., and Wang, T.: Atmospheric Peroxides in
 634 a Polluted Subtropical Environment: Seasonal Variation, Sources and Sinks, and Importance of
 635 Heterogeneous Processes, *Environmental Science & Technology*, 48, 1443–1450,
 636 <https://doi.org/10.1021/es403229x>, 2014.

637 Hoops, S., Sahle, S., Gauges, R., Lee, C., Pahle, J., Simus, N., Singhal, M., Xu, L., Mendes, P.,
 638 and Kummer, U.: COPASI—a COmplex PAthway SIMulator, *Bioinformatics*, 22, 3067–3074,
 639 <https://doi.org/10.1093/bioinformatics/btl485>, 2006.

640 Kanakidou, M., Myriokefalitakis, S., and Tsigaridis, K.: Aerosols in atmospheric chemistry and
 641 biogeochemical cycles of nutrients, *Environmental Research Letters*, 13, 063004,
 642 <https://doi.org/10.1088/1748-9326/aabcbd>, 2018.

643 Kremer, M. L.: The Fenton Reaction. Dependence of the Rate on pH, *The Journal of Physical*
 644 *Chemistry A*, 107, 1734–1741, <https://doi.org/10.1021/jp020654p>, 2003.

645 Long, Y., Charbouillot, T., Brigante, M., Mailhot, G., Delort, A.-M., Chaumerliac, N., and
 646 Deguillaume, L.: Evaluation of modeled cloud chemistry mechanism against laboratory
 647 irradiation experiments: The H_xO_y/iron/carboxylic acid chemical system, *Atmospheric*
 648 *Environment*, 77, 686–695, <https://doi.org/10.1016/j.atmosenv.2013.05.037>, 2013.

649 Mace, K. A., Kubilay, N., and Duce, R. A.: Organic nitrogen in rain and aerosol in the eastern
 650 Mediterranean atmosphere: An association with atmospheric dust, *Journal of Geophysical*
 651 *Research: Atmospheres*, 108, <https://doi.org/10.1029/2002JD002997>, 2003.

652 Marion, A., Brigante, M., and Mailhot, G.: A new source of ammonia and carboxylic acids in
 653 cloud water: The first evidence of photochemical process involving an iron-amino acid complex,
 654 *Atmospheric Environment*, 195, 179–186, <https://doi.org/10.1016/j.atmosenv.2018.09.060>,
 655 2018.

656 Masuda, T., Nakano, S., and Kondo, M.: Rate constants for the reactions of OH radicals with
 657 the enzyme proteins as determined by the p-nitrosodimethylaniline method, *Journal of*
 658 *Radiation Research*, 14, 339–345, <https://doi.org/10.1269/jrr.14.339>, 1973.

659 Matos, J. T. V., Duarte, R. M. B. O., and Duarte, A. C.: Challenges in the identification and
 660 characterization of free amino acids and proteinaceous compounds in atmospheric aerosols: A
 661 critical review, *TrAC Trends in Analytical Chemistry*, 75, 97–107,
 662 <https://doi.org/10.1016/j.trac.2015.08.004>, 2016.

663 Motohashi, N. and Saito, Y.: Competitive Measurement of Rate Constants for Hydroxyl Radical
 664 Reactions Using Radiolytic Hydroxylation of Benzoate, *Chemical & Pharmaceutical Bulletin*,
 665 41, 1842–1845, <https://doi.org/10.1248/cpb.41.1842>, 1993.

666 Neyens, E. and Baeyens, J.: A review of classic Fenton’s peroxidation as an advanced oxidation
 667 technique, *Journal of Hazardous Materials*, 98, 33–50, [https://doi.org/10.1016/S0304-](https://doi.org/10.1016/S0304-3894(02)00282-0)
 668 [3894\(02\)00282-0](https://doi.org/10.1016/S0304-3894(02)00282-0), 2003.

669 Penteado, F., Lopes, E. F., Alves, D., Perin, G., Jacob, R. G., and Lenardão, E. J.: α -Keto Acids:
 670 Acylating Agents in Organic Synthesis, *Chemical Reviews*, 119, 7113–7278,
 671 <https://doi.org/10.1021/acs.chemrev.8b00782>, 2019.

672 van Pinxteren, M., Müller, C., Iinuma, Y., Stolle, C., and Herrmann, H.: Chemical
 673 Characterization of Dissolved Organic Compounds from Coastal Sea Surface Microlayers
 674 (Baltic Sea, Germany), *Environmental Science & Technology*, 46, 10455–10462,
 675 <https://doi.org/10.1021/es204492b>, 2012.

676 van Pinxteren, M., Zeppenfeld, S., Fomba, K. W., Triesch, N., Frka, S., and Herrmann, H.:
 677 Amino acids, carbohydrates, and lipids in the tropical oligotrophic Atlantic Ocean: sea-to-air
 678 transfer and atmospheric in situ formation, *Atmospheric Chemistry and Physics*, 23, 6571–6590,
 679 <https://doi.org/10.5194/acp-23-6571-2023>, 2023.

680 Rachmilovich-Calis, S., Masarwa, A., Meyerstein, N., Meyerstein, D., and van Eldik, R.: New
 681 Mechanistic Aspects of the Fenton Reaction, *Chemistry – A European Journal*, 15, 8303–8309,
 682 <https://doi.org/10.1002/chem.200802572>, 2009.

683 Renard, P., Brissy, M., Rossi, F., Lereboure, M., Jaber, S., Baray, J.-L., Bianco, A., Delort,
 684 A.-M., and Deguillaume, L.: Free amino acid quantification in cloud water at the Puy de Dôme
 685 station (France), *Atmospheric Chemistry and Physics*, 22, 2467–2486,
 686 <https://doi.org/10.5194/acp-22-2467-2022>, 2022.

687 Samavat, S., Gholami, N., and Nazari, K.: Complexation of Iron (III) With Citrate and Tartarate
 688 Anions in Perturbed Aqueous Solutions Using Potentiometry and Difference UV/Vis. and IR
 689 Spectrophotometric Methods., *Acta Chimica Slovenica*, 54, 2007.

690 Samy, S., Robinson, J., and Hays, M. D.: An advanced LC-MS (Q-TOF) technique for the
 691 detection of amino acids in atmospheric aerosols, *Analytical and Bioanalytical Chemistry*, 401,
 692 3103–3113, <https://doi.org/10.1007/s00216-011-5238-2>, 2011.

693 Scheres Firak, D., Schaefer, T., Senff, P., Cheng, P., Sarakha, M., Brigante, M., Mailhot, G.,
 694 and Herrmann, H: Fenton-like Reactions in Acidic Environments: New Mechanistic Insights
 695 and Implications to Atmospheric Particle-Phase Chemistry., *ACS ES&T Air*, accepted
 696 manuscript, <https://doi.org/10.1021/acseistair.5c00077>, 2025.

697 Shulman, M. L., Charlson, R. J., and James Davis, E.: The effects of atmospheric organics on
 698 aqueous droplet evaporation, *Journal of Aerosol Science*, 28, 737–752,
 699 [https://doi.org/10.1016/S0021-8502\(96\)00469-7](https://doi.org/10.1016/S0021-8502(96)00469-7), 1997.

700 von Sonntag, C. and Schuchmann, H.-P.: The Elucidation of Peroxyl Radical Reactions in
 701 Aqueous Solution with the Help of Radiation-Chemical Methods, *Angewandte Chemie*
 702 International Edition in English, 30, 1229–1253, <https://doi.org/10.1002/anie.199112291>, 1991.

703 Soriano-Molina, P., García Sánchez, J. L., Alfano, O. M., Conte, L. O., Malato, S., and Sánchez
 704 Pérez, J. A.: Mechanistic modeling of solar photo-Fenton process with Fe³⁺-EDDS at neutral
 705 pH, *Applied Catalysis B: Environmental*, 233, 234–242,
 706 <https://doi.org/10.1016/j.apcatb.2018.04.005>, 2018.

707 Sorooshian, A., Wang, Z., Coggon, M. M., Jonsson, H. H., and Ervens, B.: Observations of
 708 Sharp Oxalate Reductions in Stratocumulus Clouds at Variable Altitudes: Organic Acid and
 709 Metal Measurements During the 2011 E-PEACE Campaign, *Environmental Science &*
 710 *Technology*, 47, 7747–7756, <https://doi.org/10.1021/es4012383>, 2013.

711 Strathmann, T. J. and Stone, A. T.: Reduction of Oxamyl and Related Pesticides by FeII:
 712 Influence of Organic Ligands and Natural Organic Matter, *Environmental Science &*
 713 *Technology*, 36, 5172–5183, <https://doi.org/10.1021/es0205939>, 2002.

714 Sun, L., Wu, C.-H., and Faust, B. C.: Photochemical Redox Reactions of Inner-Sphere
 715 Copper(II)-Dicarboxylate Complexes: Effects of the Dicarboxylate Ligand Structure on
 716 Copper(I) Quantum Yields, *The Journal of Physical Chemistry A*, 102, 8664–8672,
 717 <https://doi.org/10.1021/jp982045g>, 1998.

Tilgner, A., Bräuer, P., Wolke, R., and Herrmann, H.: Modelling multiphase chemistry in deliquescent aerosols and clouds using CAPRAM3.0i, *Journal of Atmospheric Chemistry*, 70, 221–256, <https://doi.org/10.1007/s10874-013-9267-4>, 2013.

Triesch, N., van Pinxteren, M., Salter, M., Stolle, C., Pereira, R., Zieger, P., and Herrmann, H.: Sea Spray Aerosol Chamber Study on Selective Transfer and Enrichment of Free and Combined Amino Acids, *ACS Earth and Space Chemistry*, 5, 1564–1574, <https://doi.org/10.1021/acsearthspacechem.1c00080>, 2021.

Vel Leitner, N. K., Berger, P., and Legube, B.: Oxidation of Amino Groups by Hydroxyl Radicals in Relation to the Oxidation Degree of the α -Carbon, *Environ. Sci. Technol.*, 36, 3083–3089, <https://doi.org/10.1021/es0101173>, 2002.

Wang, T. L., Tong, H. W., Yan, X. Y., Sheng, L. Q., Yang, J., and Liu, S. M.: Determination of Volatile Carbonyl Compounds in Cigarette Smoke by LC-DAD, *Chromatographia*, 62, 631–636, <https://doi.org/10.1365/s10337-005-0675-8>, 2005.

Wang, Z., Chen, X., Ji, H., Ma, W., Chen, C., and Zhao, J.: Photochemical Cycling of Iron Mediated by Dicarboxylates: Special Effect of Malonate, *Environmental Science & Technology*, 44, 263–268, <https://doi.org/10.1021/es901956x>, 2010.

Weller, C., Horn, S., and Herrmann, H.: Photolysis of Fe(III) carboxylato complexes: Fe(II) quantum yields and reaction mechanisms, *Journal of Photochemistry and Photobiology A: Chemistry*, 268, 24–36, <https://doi.org/10.1016/j.jphotochem.2013.06.022>, 2013.

Yuan, Y., Feng, L., Xie, N., Zhang, L., and Gong, J.: Rapid photochemical decomposition of perfluorooctanoic acid mediated by a comprehensive effect of nitrogen dioxide radicals and $\text{Fe}^{3+}/\text{Fe}^{2+}$ redox cycle, *Journal of Hazardous Materials*, 388, 121730, <https://doi.org/10.1016/j.jhazmat.2019.121730>, 2020.